Simple physics-based adjustments reconcile the results of Eulerian and Lagrangian techniques for moisture tracking

Alfredo Crespo-Otero[1], Damián Insua-Costa[2], Emilio Hernández-García[3], Cristóbal López[3] and Gonzalo Míguez-Macho[1]

[1]CRETUS, Non-linear Physics Group, Universidade de Santiago de Compostela, Galicia, Spain
[2]Hydro-Climate Extremes Lab (H-Cel), Ghent University, Ghent, 9000, Belgium
[3]Instituto de Física Interdisciplinar y Sistemas Complejos (IFISC), CSIC-UIB, Campus Universitat de les Illes Balears, 07122, Palma de Mallorca, Spain

Correspondence to: Alfredo Crespo-Otero (alfredocrespo.otero@usc.es)

Abstract. The increase in the number and quality of numerical moisture tracking tools has greatly improved our understanding of the hydrological cycle in recent years. However, the lack of observations has prevented a direct validation of these tools, and it is common to find large discrepancies among the results produced by them, especially between Eulerian and Lagrangian methodologies. Here, we evaluate two diagnostic tools for moisture tracking, WaterSip and UTrack, using simulations from the Lagrangian model FLEXPART. We assess their performance against the Weather Research and Forecasting (WRF) model with Eulerian Water Vapor Tracers (WRF-WVTs). Assuming WRF-WVTs results as a proxy for reality, we explore the discrepancies between the Eulerian and Lagrangian approaches for five precipitation events associated with atmospheric rivers and propose some physics-based adjustments to the Lagrangian tools. Our findings reveal that UTrack, constrained by evaporation and precipitable water data, has a slightly better agreement with WRF-WVTs than WaterSip, constrained by specific humidity data. As in previous studies, we find a negative bias in the contribution of remote sources, such as tropical ones, and an overestimation of local contributions. Quantitatively, the root-mean-square-error (RMSE) for contributions from selected source regions is 5.55 for WaterSip and 4.64 for UTrack, highlighting UTrack's narrowly superior performance. Implementing our simple and logical corrections leads to a significant improvement in both methodologies, effectively reducing the RMSE by over 50 % and bridging the gap between Eulerian and Lagrangian outcomes. Our results suggest that the major discrepancies between the different methodologies were not rooted in their inherently different nature, but in the obviation of basic physical considerations that may be easily straightened out.

1 Introduction

Water is one of Earth's most important resources, and its availability and distribution are crucial to the future of the different ecosystems, including humans. Given its importance and scarcity, it is vital to understand how water is transported between different regions of our planet (Oki and Kanae, 2006). Water can be transported within a catchment through rivers and groundwater flow. However, the transport of water between basins, or from ocean to land, is mostly done via the

atmosphere, through what is known as the atmospheric branch of the water cycle. To investigate the latter, researchers have developed different moisture tracking methods that make it possible to analyse where moisture contributing to precipitation has previously evaporated (see Gimeno et al., 2012, for a review). Apart from analytical approaches (Dominguez et al., 2006; Rios-Entenza and Miguez-Macho, 2014; Trenberth, 1999), the most used models to this end are numerical or

35   computational routines. Within this group, two main classes can be distinguished: Eulerian water vapor tracers, e.g., (Insua-Costa and Miguez-Macho, 2018; Koster et al., 1986; Sodemann and Stohl, 2009), and Lagrangian transport models, (Dirmeyer and Brubaker, 1999; Sodemann et al., 2008; Stohl and James, 2004). The classification can be based on alternative criteria, e.g. whether the moisture tracking is performed simultaneously with the computation of meteorological fields, such as wind or specific humidity (online), or not (offline). Additionally, the tracking can be either forward or

40   backward, depending on whether the moisture is tracked forward or backward in time. Despite the diversity of methodologies, most academics often use a single model, and the few works in which multiple methods have been tested show that results can be highly discrepant, (Cloux et al., 2021; van der Ent et al., 2013; Winschall et al., 2014).

The aforementioned techniques have been particularly used to identify moisture sources in precipitation events associated

45   with atmospheric rivers (ARs). ARs are structures of enhanced moisture and intense water vapor transport in the atmosphere, typically located in the pre-cold frontal region of an extratropical cyclone (Gimeno et al., 2014), which can eventually cause extreme rainfall (Ralph et al., 2006). However, few studies address this problem with a moisture tracking methodology, e.g., (Eiras-Barca et al., 2017; Hu and Dominguez, 2019; Liberato et al., 2013; Ramos et al., 2016), and even fewer go beyond the identification of moisture sources to quantify them.

50

In this context, the goal of this paper is to compare and adjust two Lagrangian methodologies for the computation of moisture sources for precipitation (or precipitation sources) so that the results are aligned with those provided by the Weather Research and Forecasting (WRF) model with Water Vapor Tracers (WRF-WVTs; Insua-Costa and Miguez-Macho, 2018), focusing on AR-related rainfall events. The rationale for this approach is simple. Eulerian water vapor tracers are

55   widely considered the most accurate technique for moisture tracking because, being coupled to a meteorological model, they consider in detail all the physical processes that affect moisture in the atmosphere. Their disadvantage, however, is that they are computationally expensive, and therefore their application over long time periods or in many case studies is often unfeasible. In contrast, Lagrangian methods involve more uncertainty but are much more computationally efficient. Achieving a Lagrangian moisture tracking methodology that mimics the WRF-WVTs results would therefore imply having a

60   very accurate and at the same time flexible tool that can be applied to a large number of ARs, our goal for the future, but also to other types of weather or climate phenomena. Importantly, WRF-WVTs have been fully validated (Insua-Costa and Miguez-Macho, 2018), showing an almost exact performance within the "model world", so that, in the absence of direct observations, we believe that the results provided by WRF-WVTs are particularly suitable to be considered as synthetic observations when comparing with other methods.

65

The strategy of using water vapor tracers as ground truth versus Lagrangian models has been previously used in several studies. For example, in van der Ent et al., (2013) the outcomes of a tagging tool implemented in the MM5 model are taken as ground truth to analyse two other offline methods. Winschall et al., (2014) employed a moisture tagging technique integrated into the COSMO weather prediction model as ground truth to evaluate the WaterSip method (Sodemann et al.,

70   2008), which used trajectories from the Lagrangian particle dispersion model FLEXPART (Pisso et al., 2019). More recently, Cloux et al., (2021) used this same Lagrangian diagnostic tool to compute precipitation sources, but with trajectories generated with FLEXPART-WRF (Brioude et al., 2013), and compared the results with those of WRF-WVTs. However, these previous studies were limited to highlighting the large discrepancies between the results provided by Lagrangian and Eulerian tools, but they did not provide improvements that would reconcile the different methodologies.

75

In our case, the FLEXPART-WRF model is employed to generate back trajectories of air parcels contributing to precipitation in five AR events, and we assess two of the most widely used Lagrangian diagnostic tools for estimating moisture sources: WaterSip and UTrack (Tuinenburg and Staal, 2020). Our focus is on understanding the origins of discrepancies between the outcomes of these methodologies and those derived from WRF-WVTs, with the aim of

80   introducing physics-based adjustments to them that minimize these differences. Our framework is particularly well suited for this validation, as both the moisture tracking with WRF-WVTs and with FLEXPART-WRF are driven by the same WRF-simulated atmospheric fields. Additionally, we validate the proposed modifications under a different scenario where trajectories are computed using FLEXPART forced with data from the ERA5 reanalysis (Hersbach et al., 2020), instead of WRF. We do this because the vast majority of FLEXPART users, as well as users of other Lagrangian models, force their

85   simulation with reanalysis data.

In what follows, we first present the AR cases studied (Section 2.1) and the Eulerian and Lagrangian methodologies used to calculate precipitation sources (Sect. 2.2 and Sect. 2.3). Section 3 then includes a series of analysis, focusing on the comparison of the results produced by the Lagrangian methodologies with those provided by the WRF-WVTs model.

90   Finally, Sect. 4 provides a summary and the conclusions of this work.

2 Methods

2.1 Selected AR cases

In this section we introduce the five precipitation events selected, all of them caused by the landfall of an AR and well documented in the literature. We chose cases from all over the world, not just from a specific region. In Fig. 1 we show both

95   the integrated water vapor and accumulated precipitation fields from WRF simulations (see Sect. 2.2) for these
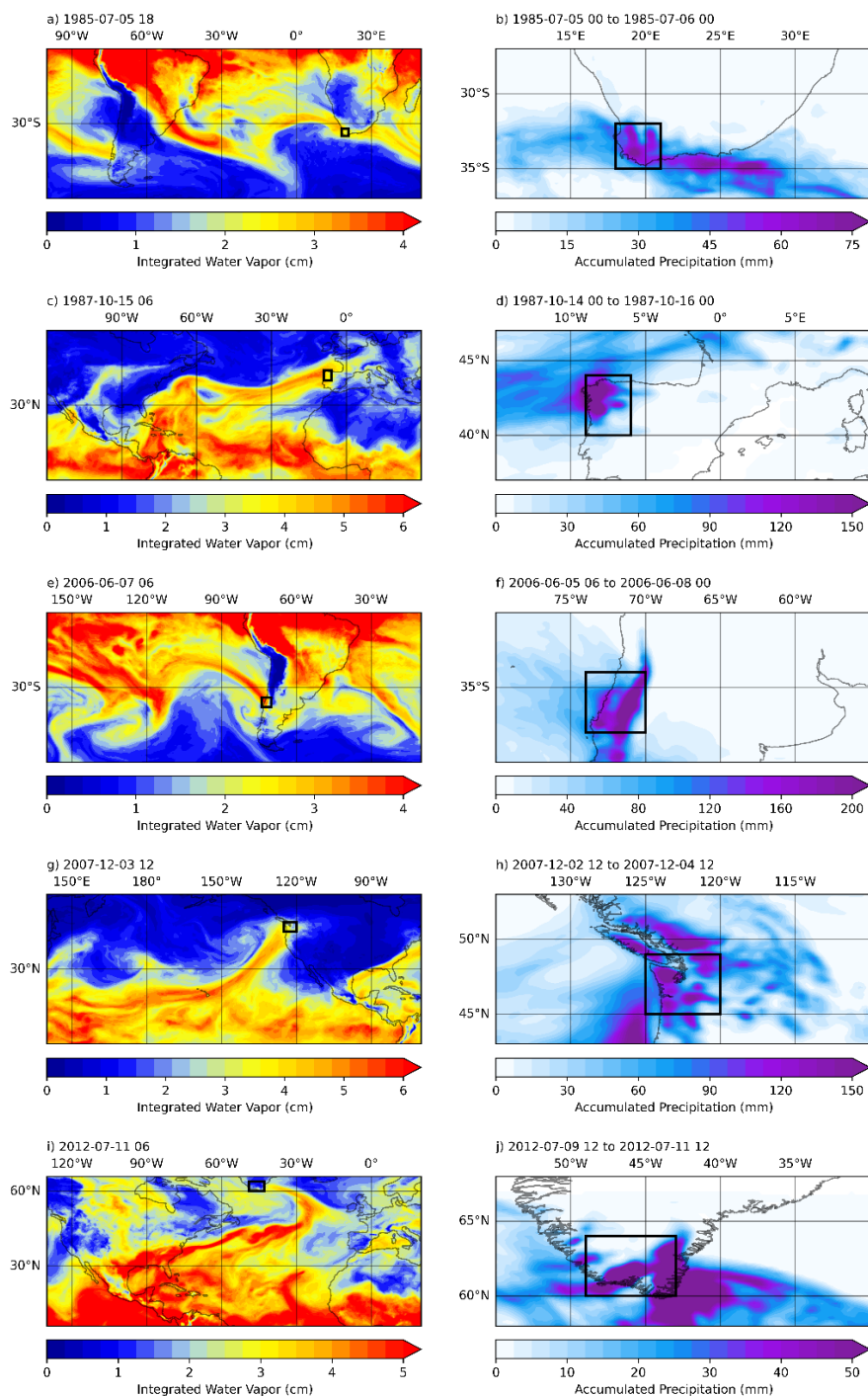
Figure 1: Integrated water vapor during the selected AR-related precipitation events (left) and accumulated precipitation during the entire rainfall episodes (right). The black boxes are the regions in which precipitation will be tracked.

cases. Black boxes in this figure highlight the areas most affected by rainfall (Table 1). A more detailed description of these

100 episodes can be found in Sect. S1 in the Supplement.

t_i	Δt (h)	λ_1 (°)	λ_2 (°)	ϕ_1 (°)	ϕ_2 (°)
1985-07-05 00	55	-35.0	-32.0	18.0	21.0
1987-10-14 00	49	40.0	44.0	-9.0	-6.0
2006-06-05 06	67	-38.0	-34.0	-74.0	-70.0
2007-12-02 12	49	45.0	49.0	-125.0	-120.0
2007-12-09 12	49	60.0	64.0	-49.0	-43.0

Table 1: Starting date and time (t_i) and duration (Δt) of the rainfall events associated to the five ARs studied, together with the coordinates defining the region where precipitation will be tracked (black boxes in Fig. 1): λ_1, λ_2 (latitudes) and ϕ_1, ϕ_2 (longitudes).

105

The first rainfall event considered affected South Africa in July 1985. Figure 1a and 1b clearly show that the event was

linked to an AR, as already indicated by other authors (Blamey et al., 2018). The second AR affected the northwest region of

the Iberian Peninsula (Fig. 1c and 1d) and was associated with the infamous extratropical cyclone coined as the "Great

Storm" for the catastrophic impacts it caused in the United Kingdom. Moisture sources for this AR-related precipitation

110 event were previously analysed using the WRF-WVTs tool in Eiras-Barca et al., (2017). The third case selected corresponds

to an AR that impacted central Chile and the Andes (Fig. 1e and 1f), resulting in floods and damage in the region, and was

analysed in Viale et al., (2013). The fourth AR considered (Fig. 1g and 1h) was associated with the well-known Great

Coastal Gale of 2007, affecting the US West Coast. The moisture sources for this event were also investigated in Eiras-Barca

et al., (2017) using the WRF-WVTs model. Finally, the last AR studied hit Greenland (Fig. 1i and 1j) leading to a severe ice

115 and snow melting episode, (Mattingly et al., 2018).

2.2 WRF-WVTs

As previously mentioned, the moisture tracking model used as a proxy for reality in this study is WRF-WVTs, (Insua-Costa

and Miguez-Macho, 2018), a moisture tagging tool implemented in the WRF model version 4.3.3, (Skamarock et al., 2021).

Here WRF is run at a spatial resolution of 20 km and 38 vertical levels in two different semi-hemispherical domains (Fig. 2),

120 depending on whether the AR of study occurs in the northern or southern hemisphere. Initial and boundary conditions come

from the ERA5 reanalysis. We use a spectral nudging technique (Miguez-Macho et al., 2004) to prevent large-scale

atmospheric fields from deviating significantly from the reanalysis. Spectral nudging ensures an accurate representation of

the atmosphere throughout the simulation period, even several days after the simulation has started. This aspect is

particularly important in our tracking experiments, since we start our simulations 30 days before the beginning of the rainfall

125   episode (Table 1) to allow enough time for the moisture to evaporate. The underlying reason for this long spin-up time is that

probability density functions for atmospheric residence time of water vapor are positively skewed (van der Ent et al., 2013).

The WRF-WVTs tool is an Eulerian, online and forward moisture tracking technique, as the water vapor tracers are coupled

to the meteorological model, and the latter needs to be run forward in time. As clarified in Insua-Costa et al., (2022), to track

130   moisture coming from a source region S in the WRF-WVTs framework it is necessary to modify the source term in the WRF

prognostic equation for moisture (QFX):

$$TRQFX = QFX \cdot M, \tag{1}$$

where M is a binary array designating the region S with values of 1 and the rest with 0. In our case QFX does not come from

the evaporative flux simulated by WRF land surface scheme, but we assimilate it from the ERA5 reanalysis. Specifically, if

135   E represents the assimilated evaporation interpolated onto the model grid, ρ_w denotes the water density and ΔT is the time

interval in the reanalysis, then the moisture flux from the surface QFX can be expressed as:

$$QFX = -\frac{\rho_\mathrm{w} E}{\Delta T}. \tag{2}$$

The negative sign accounts for the different criteria for positive surface fluxes between WRF and ERA5. If ΔT were large, a

time interpolation would also be needed. Finally, the tool tracks moisture until it precipitates, so a new variable representing

140   tracer precipitation, i.e. originating from the source region S is defined (TP_S). Consequently, the fraction of rainfall in a

specific region R coming from S can be determined as

$$F_S = \frac{\sum_{i,j} TP_S(i,j)}{\sum_{i,j} P(i,j)} \forall (i,j) \in R, \tag{3}$$

where P is total precipitation and regions R for the different ARs are defined in Table 1 and plotted in Fig. 1 as black boxes.

145   WRF-WVTs can track not only moisture evaporated from S, but also moisture advected from S, by changing the evaporative

flux QFX by the specific humidity q in Eq. (1). In this case the source is three dimensional (3-D) and in the former, two-

dimensional (2-D). We consider 11 source regions in each domain (Fig. 2), selected to maximize the contribution from the 2-

D sources (nine in total). We only use two 3-D sources at the model domain boundaries, in order to track all moisture

originating from outside the model domain (red lines in Fig. 2). For additional information on the WRF-WVTs simulations,

150   we refer to Sect. S2 in the Supplement.
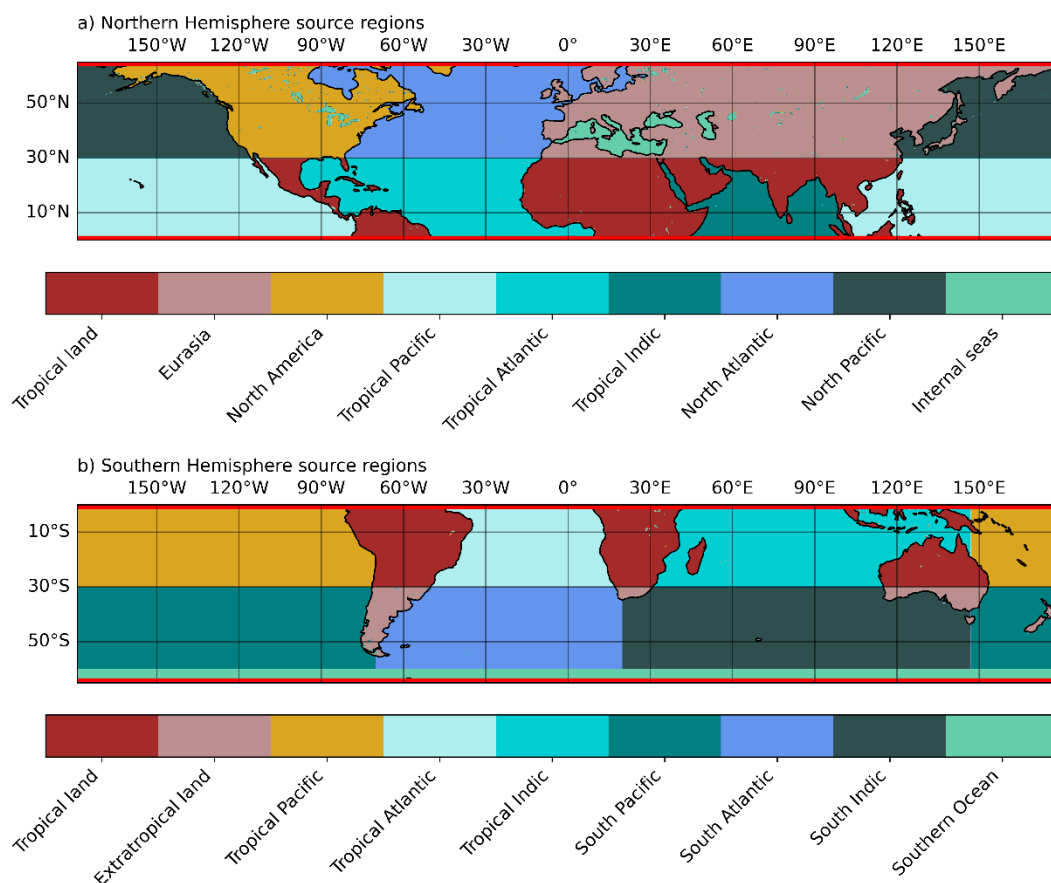
Figure 2: The two simulation domains and the nine 2D moisture sources analysed for each of them, along with the two 3-D sources at the domain boundaries (red lines). Northern Hemisphere cases use the configuration in a), while Southern Hemisphere ones use that in b).

2.3 Lagrangian techniques

The two Lagrangian moisture tracking methods we use, as previously commented, operate as post-processing routines for the Lagrangian particle dispersion model FLEXPART (Pisso et al., 2019), widely utilized in studies dedicated to understanding the origin and transport of atmospheric humidity (Drumond et al., 2014; Ramos et al., 2016; Sodemann and Stohl, 2009). This model is prepared to ingest input data from the European Centre for Medium-Range Weather Forecasts (ECMWF) Integrated Forecast System (IFS) and the United States National Center of Environmental Prediction (NCEP) Global Forecast System (GFS). Additionally, an adapted version of FLEXPART, known as FLEXPART-WRF (Brioude et al., 2013), is enabled to process output data from the WRF model. We will start using FLEXPART-WRF and then extend our comparison with WRF-WVTs to FLEXPART constrained with ERA5. Both FLEXPART and FLEXPART-WRF provide hourly information about the 3-D position, specific humidity, pressure, density and temperature of the parcel, together with

165 the atmospheric boundary layer (ABL) height. Except for the position and the ABL height, the other variables are obtained by interpolating ERA5 or WRF to the position of the parcels. While FLEXPART-WRF input data were described in the previous section (WRF 3-hourly output data), in our case FLEXPART assimilates hourly data from the ERA5 reanalysis on a $0.5° \times 0.5°$ grid and across the 70 vertical model levels closest to the surface. Additional details about FLEXPART and FLEXPART-WRF simulations are given in Sect. S2 in the Supplement.

170

The first Lagrangian methodology we employ, WaterSip, was introduced by Sodemann et al., (2008), and it is now implemented in several moisture tracking frameworks (Fernández-Alvarez et al., 2022; Keune et al., 2022). It starts by assuming that the atmospheric column over the region where precipitation occurs is filled with air parcels, and that their trajectories contain information about their location and specific humidity for the previous days, in our case 30 days. For

175 each parcel WaterSip calculates the contribution of the moisture gained at each time step to the amount of water that the parcel loses in the last iteration. This loss is then assumed to represent the observed precipitation when aggregated over all parcels. Although both FLEXPART and FLEXPART-WRF output are hourly, we only use 3-hourly data, since a very high temporal resolution can introduce noise into the WaterSip diagnostic, leading to systematic biases (see Fig. S7 in the Supplement for further details).

180

More specifically, the WaterSip method begins by identifying where each parcel uptakes water, by computing the difference in specific humidity between consecutive time steps, $\Delta q_{\text{parcel},t} = q(\vec{r}_{\text{parcel},t}, t) - q(\vec{r}_{\text{parcel},t-1}, t-1)$. A positive difference is interpreted as evaporation, while a decrease in humidity is linked to precipitation. This interpretation relies on the following approximation for the surface freshwater flux *E-P* in a given area *A*, introduced by Stohl and James, (2004):

185 $$E - P \approx \frac{1}{A} \sum_{\text{parcel} \in A} m_{\text{parcel}} \frac{\Delta q_{\text{parcel},t}}{\Delta t},$$ (4)

where m_{parcel} is the parcel mass. In Sodemann et al., (2008), apart from the specific humidity increase, additional criteria are imposed to determine whether a moisture uptake is actually occurring or not. These are (1) requiring that the specific humidity increase exceeds a minimum threshold, that we set here to $\Delta q = 0.05$ g kg⁻¹, and (2) it occurs within the ABL. This ensures that moisture increases above the ABL are not attributed to surface evaporation. Both filters were introduced to

190 eliminate noise and non-physical increments. However, some subsequent studies (e.g., Fremme and Sodemann, 2019) have ignored the ABL filter, arguing that parcels above the ABL can still be indirectly influenced by surface evaporation through moist convection or turbulence. Therefore, we refer to the basic WaterSip configuration as the one in which only criterion (1) applies.

195 Once the uptake points are identified, the contribution of each positive moisture increment is initialized to $\Delta q_{\text{parcel},t}$ and linked to the uptake point, calculated as the mid-point of the parcel position $(\vec{r}_{\text{parcel},t} + \vec{r}_{\text{parcel},t-1})/2$. The method then proceeds forward in time, applying a discounting procedure when a decrease in specific humidity is observed. This

procedure involves reducing previous contributions proportionally to the amount of water remaining in the parcel originating from these contributions. Specifically, if $t' > t$ corresponds to the first specific humidity decrease after t for a given parcel

200 ($\Delta q_{\text{parcel},t'} < 0$), the initial contribution $\Delta q_{\text{parcel},t}$ is updated and reduced to $\Delta q_{\text{parcel},t}^{t'}$ as follows:

$$\Delta q_{\text{parcel},t}^{t'} = \Delta q_{\text{parcel},t} \left(1 + \frac{\Delta q_{\text{parcel},t'}}{q\left(\vec{r}_{\text{parcel},t'-1},t'-1\right)} \right). \tag{5}$$

After reaching the most recent time step, a spatial distribution for the moisture origin of each parcel is obtained. The final stage of the methodology involves selecting only those parcels that contribute to precipitation and weighting the spatial distributions by the final humidity loss. For the selection of these parcels, a threshold of 80% is applied to the relative

205 humidity (RH), ensuring the exclusion of unsaturated parcels that could hardly have contributed to the precipitation.. Obviously, parcels with a final humidity increase are also discarded. For a detailed mathematical description of the method, see Sect. S3.1 in the Supplement.

The second type of trajectory-based moisture tracking method we employ was originally introduced by Dirmeyer and

210 Brubaker, (1999), and is currently widely used in the framework of the UTrack-atmospheric-moisture tool (Tuinenburg and Staal, 2020). Instead of the more common forward version, here we use the backward one (Staal and Koren, 2023). Unlike WaterSip, UTrack does not attribute moisture sources based on the specific humidity of air parcels, but using evaporation and precipitable water fields. When evaporation occurs at a parcel's location, a fraction of its moisture (equal to the ratio of evaporation to precipitable water) is attributed to that location, and the parcel's moisture content is updated accordingly. This

215 process continues until 99 % of the parcel's moisture has been allocated, with a maximum duration of 30 days in our case. At the end of the calculation, a spatial distribution for the moisture origin of each parcel is obtained, similar to WaterSip. When aggregating results from all parcels, as all of them account for total rainfall amount, the precipitation sources are obtained. An important difference with WaterSip is that in this case the contribution of each parcel is weighted by the humidity profile, instead of the water lost in the last time step. Another difference with WaterSip is that UTrack performs the calculation of

220 the parcel trajectories itself. However, we use an adaptation of UTrack to work with FLEXPART and FLEXPART-WRF trajectories. For a detailed explanation of this method, we again refer to Sect. S3.1 in the Supplement.

Finally, in order to compare WaterSip and UTrack with WRF-WVTs, their output fields - representing the amount of evaporated water resulting in precipitation - must be aggregated to the selected source regions and then divided by total

225 precipitation, in order to calculate the rainfall fractions F_S, as in Eq. (2). This allows us to assess each Lagrangian model by using the Root Mean Square Error,

$$\text{RMSE}_m = \sqrt{\frac{1}{N} \sum_{i=1}^{N} \left(F_{S_i}^{\text{WVTs}} - F_{S_i}^{m} \right)^2}, \tag{6}$$

where N is the number of sources and $F_{S_i}^{\text{WVTs}}$, $F_{S_i}^m$ the precipitation fractions for WRF-WVTs and for the evaluated Lagrangian model, respectively. Given that this metric is very sensitive to outliers, the Mean Absolute Error (MAE) and its

230 associated score, the Mean Absolute Error Skill Score (MAESS), are also used to obtain an average rating:

$$\text{MAE}_m = \frac{1}{N}\sum_{i=1}^{N}\left|F_{S_i}^{\text{WVTs}} - F_{S_i}^m\right|, \quad \text{MAESS} = 1 - \frac{\text{MAE}_m}{\text{MAE}_r}, \tag{7}$$

Where MAE_r is the MAE if all rainfall fractions were equal to $1/N$. Note that we use the MAESS and not the coefficient of determination as skill score because the latter leads to negative values in our analysis, and this can be problematic when averaging over all AR cases.

3. Results

In this section the main results of this study are presented. In Sect. 3.1 the most basic configurations of WaterSip and UTrack are assessed by comparing their outputs with those provided by the WRF-WVTs tool. Next, in Sect. 3.2 some physics-based adjustments are introduced in the Lagrangian methodologies with the intention of minimising the discrepancies with the WRF-WVTs results. Finally, in Sect. 3.3 we test the introduced modifications when the trajectories are generated by

240 FLEXPART, with input data from the ERA5 reanalysis.

3.1 Basic results for WRF-WVTs vs WaterSip and UTrack

Figure 3 illustrates the rainfall fractions from WRF-WVTs for the five precipitation events introduced before, and for the eleven source regions considered. The results are categorized into Northern Hemisphere and Southern Hemisphere cases, as the selected source regions are identical for ARs occurring in the same hemisphere. For the Iberian Peninsula, US West

245 Coast, and South Africa events, the most important contributions are from the extratropical oceanic areas where the ARs developed. Conversely, in the Andes case the primary contribution is from the Tropical Pacific. In these four cases, more than 75 % of the precipitation originates from oceanic sources. However, a different pattern is observed in the Greenland case, where there is a remarkable continental contribution from North America, reducing the oceanic precipitation fraction to below 50 %. This is consistent with previous studies showing that ARs in polar regions can exhibit unique features (Guan

250 and Waliser, 2019) and that moisture sources in AR-related precipitation events can be highly variable.

As depicted in Figure 3, the Eulerian WRF-WVTs technique does not account for 100 % of the precipitation. This is because a small portion of the rain may originate from evaporation that occurred more than 30 days before the precipitation event. This fraction of rain with untraceable origins by WRF-WVTs varies from case to case. Since both Lagrangian models

255 typically attribute the entire 100 % of precipitation in their basic configurations, we will scale the results shown in Figure 3 for comparison purposes. In cases where WaterSip or UTrack do not account for 100 % of the precipitation, the bias will also be calculated after adjusting for these precipitation fractions.
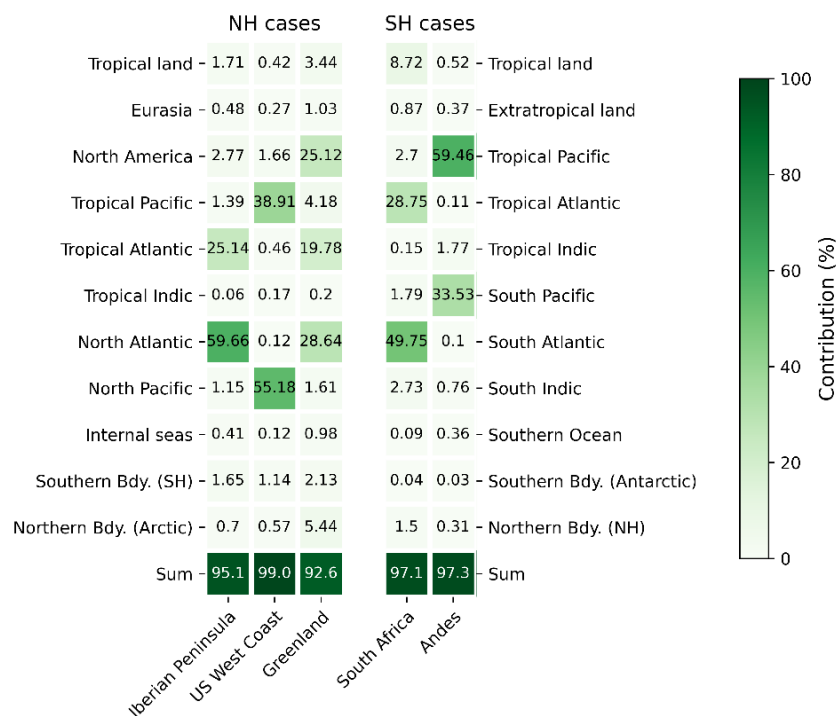
Figure 3: Precipitation fractions (%) in the different rainfall events originating from the selected sources, computed using the WRF-WVTs model. To the left, Northern Hemisphere (NH) cases. To the right, Southern Hemisphere (SH) cases. The last row shows the sum of all contributions.

We start the comparison with WRF-WVTs by using the most basic configurations of the WaterSip and UTrack diagnostic tools, described in Sect. 2.3. Figure 4a presents the results for the WaterSip diagnostic tool. A significant bias is observed in certain contributions, particularly evident in those of the main tropical and extratropical oceanic source regions for each case. There is a clear tendency for WaterSip to underestimate tropical and overestimate extratropical contributions, something that has already been observed in previous studies (Cloux et al., 2021; Winschall et al., 2014). For the Iberian Peninsula, South Africa and Andes cases, biases are high for the main sources, of around 10 %, with a RMSE (see Fig. 5) of 4.51, 5.77 and 3.29, respectively. The Greenland case presents worse results, as WaterSip overestimates the fraction of precipitation originating from the North Atlantic by more than 40 %, leading to a RMSE of 13.5. However, the US West Coast case does show good results, with a maximum bias of 1.54% in the Tropical Pacific contribution and a RMSE of 0.72. Overall, the average RMSE is 5.55, while the average MAESS is 0.70 (see Table S1 in the Supplement).

Fig. 4b displays the results for the UTrack methodology. The lighter colors in this panel indicate a reduction in the bias of precipitation fractions compared with WaterSip results, especially for the NH cases. This improvement is reflected in the RMSE, which ranges from 2.00 in the Iberian Peninsula case to 6.26 in the South Africa case (Fig. 5). The average RMSE

for UTrack is 4.64, with an average MAESS of 0.77, indicating a better performance relative to WaterSip. However, there still persists an underestimation of tropical contributions, particularly evident in the Southern Hemisphere cases. For example, for the South Africa rainfall episode the estimated contribution from the Tropical Atlantic is 14.88, far from the 280 "true" value of 29.6 which arises from scaling the contribution shown in Fig. 3. Both the better agreement and the underestimation of tropical contributions have already been documented in the literature. Specifically, the rainfall fractions computed using the UTrack-atmospheric-moisture tool for the 2021 European floods by Staal and Koren, (2023) closely align with the WRF-WVTs fractions calculated in Insua-Costa et al., (2022), with the primary discrepancy being in the tropical contribution.
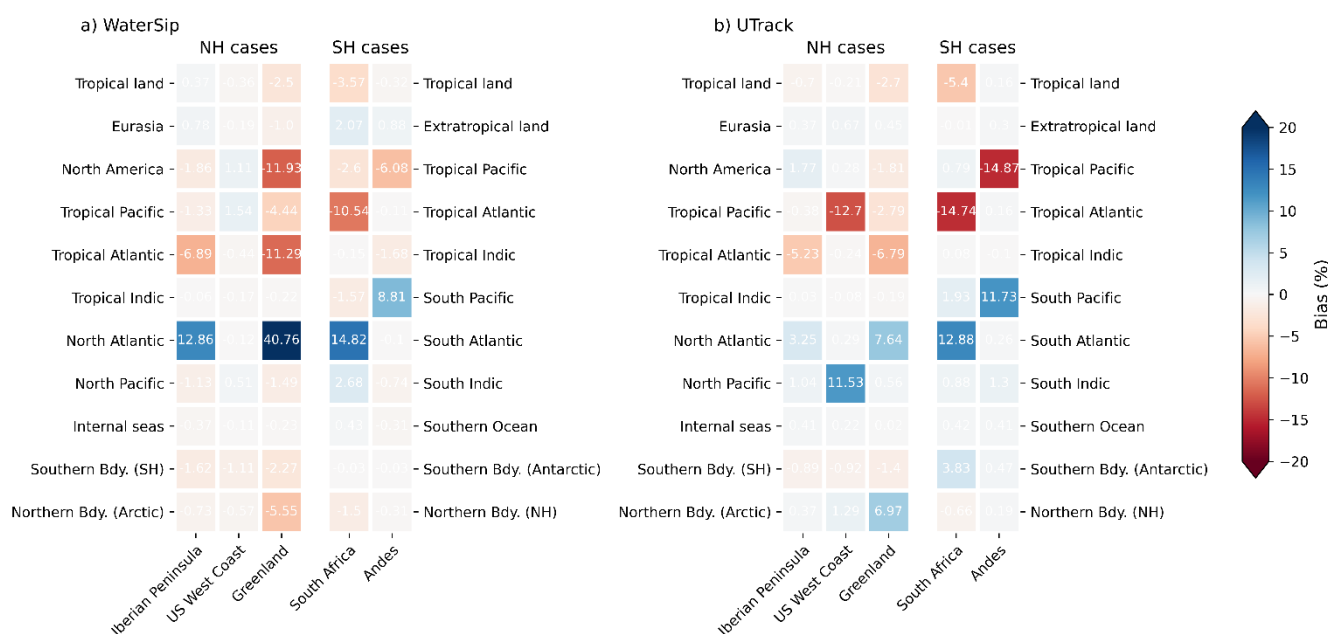
285

Figure 4: Bias in precipitation fraction (%) obtained using the basic configurations of the WaterSip and UTrack models, for trajectories generated with WRF input data (FLEXPART-WRF). Biases are computed subtracting the "true'" outcomes of WRF-WVTs from the corresponding values of WaterSip and UTrack.

3.2 Improvements in Lagrangian methodologies

290 ### 3.2.1 WaterSip

The most remarkable conclusion extracted from Fig. 4a is that WaterSip has a systematic underestimation of tropical contributions in AR-related precipitation events. While this discrepancy could be attributed to potential systematic errors in trajectory calculations, we will proceed under the assumption that these calculations are correct and instead focus on exploring the inherent capabilities of WaterSip itself to address this issue. Specifically, we conjecture that the non-physical 295 humidity fluctuations along the trajectories may account for the observed underestimation of tropical contributions and, more

broadly, of remote sources. To explain it, let us assume an air parcel that at a certain time step increased its specific humidity in 2.0 g kg⁻¹, and that it experiments a non-physical decrease of 0.05 g kg⁻¹ followed by another non-physical increase of 0.05 g kg⁻¹, such that it returns to its original value. Although these two fluctuations seem to offset each other, the original uptake of 2.0 g kg⁻¹ is now reduced to 2.0(1-0.05/2.0)=1.95 g kg⁻¹. If these fluctuations continue to occur, we are multiplying

300 the initial value by a number smaller than 1 many times (as many as 3-hour intervals in 30 days), so this original contribution clearly ends up dropping well below its true value. In other words, we hypothesize that non-physical negative changes in specific humidity penalize much earlier contributions in WaterSip, i.e. remote sources, because the error they cause accumulates over time.
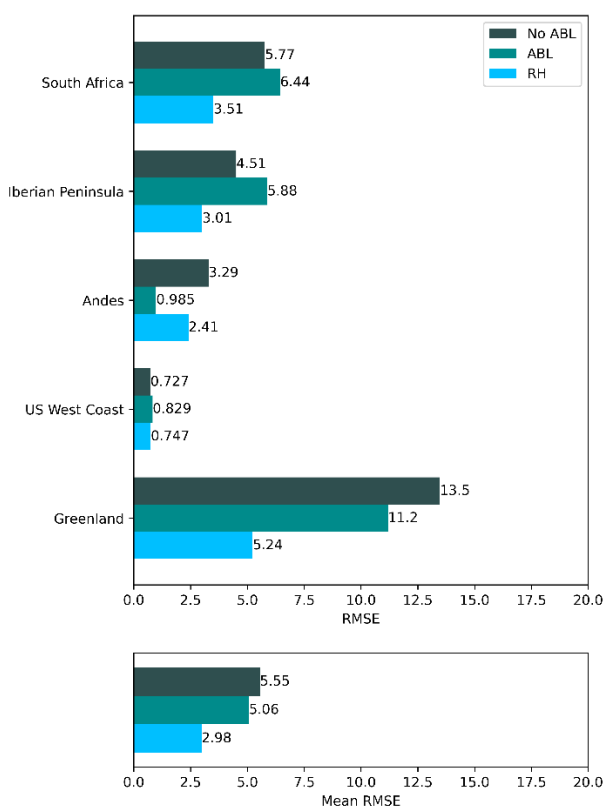
305

Figure 5: RMSE for the five AR-related precipitation events considered in this study (upper panel), and average of all of them (below). Three different configurations of the WaterSip methodology are evaluated: the most basic one (No ABL), neglecting increments above the ABL (ABL), and discarding decreases below a minimum relative humidity (RH).

310 In the past, efforts have focused on reducing spurious positive uptakes by imposing a minimum threshold in specific humidity increases and only considering moisture gains below the ABL height, as discussed in the methodology. In our case, together with the specific humidity increment threshold of $\Delta q = 0.05$ g kg⁻¹, we introduce an additional criterion to

identify non-physical decreases. We require a minimum relative humidity of 80 % immediately before a decrease in specific

humidity occurs. If this is not the case, previous contributions are not reduced due to this decrease. Interestingly, this is the

315   same criterion that is typically used to detect air parcels contributing to precipitation in the final time step (see Sect. 2.3), but

it has never been tested en-route.

Figure 5 shows the RMSE for the precipitation fractions computed using the WaterSip methodology, assuming that the true

values are those derived from WRF-WVTs (Fig. 3). The values shown by the dark green bars ("No ABL") have already been

320   discussed above as they correspond to the basic configuration of WaterSip. We now present the results also for the

configuration in which we discard moisture uptakes above the ABL height ("ABL"; light green) and for the configuration in

which we consider RH en-route ("RH"; blue). Consistent with the findings of Cloux et al., (2021), a modest improvement is

observed for the "ABL" configuration, as the average RMSE is reduced from 5.55 to 5.06. However, this behavior is not the

same for all cases, as for some of them the error increases significantly (South Africa and Iberian Peninsula cases), while in

325   the Andes case the RMSE decreases markedly from 3.29 to 0.985. In contrast, our "RH" modification results in a more

substantial improvement, as reflected by the average RMSE (2.98 versus 5.06). The improvement is especially important in

the South Africa, Iberian Peninsula and Greenland cases, where the contribution of the extratropical Atlantic was initially

overestimated by 15 %, 10 % and 40 %, respectively. When applying the proposed modification, these biases are reduced by

about 50 %. For the other two cases, the results of the original configuration were already good, and remain approximately

330   the same after applying the "RH" modification. It should be noted that these improvements could not have been obtained by

simply increasing the time step further to 6 h, as in that case the average RMSE would only drop to 5.04 (Table S2 in the

Supplement) and would slightly increase to 3.25 if combined with our proposed modification. In terms of skill score (Table

S1 in the Supplement), the "RH" configuration clearly outperforms the original and the "ABL", as the average MAESS is

significantly higher (0.84 versus 0.70 and 0.72).

335

To better illustrate these results, we further examine the moisture sources for two of the selected AR-related precipitation

events, specifically, the South Africa and Greenland cases. In Fig. 6 the precipitation sources for these events are depicted

using the WaterSip methodology. Fig. 6a and 6c (left) present the results using the basic, "No ABL", configuration, while

panels Fig. 6b and 6d (right) correspond to the "RH" experiment. Clearly, the spatial distributions of these moisture sources

340   reveal a much more pronounced dominance of local sources in the "No ABL" situation, in contrast to the "RH" setup. This is

particularly evident in the Greenland case, where in the basic configuration the moisture source field only marginally

penetrates into North America, despite being the second largest contribution according to WRF-WVTs. Conversely, the

situation improves markedly when employing the proposed relative humidity threshold. In both cases, the tropical

contributions increase and the extratropical ones decrease, coming closer to the results provided by WRF-WVTs (black and

345   red text in Fig. 6). The bias remains after the en-route relative humidity correction, but is much smaller. Analogous results

are included in Fig. S9 in the Supplement for the other rainfall events.
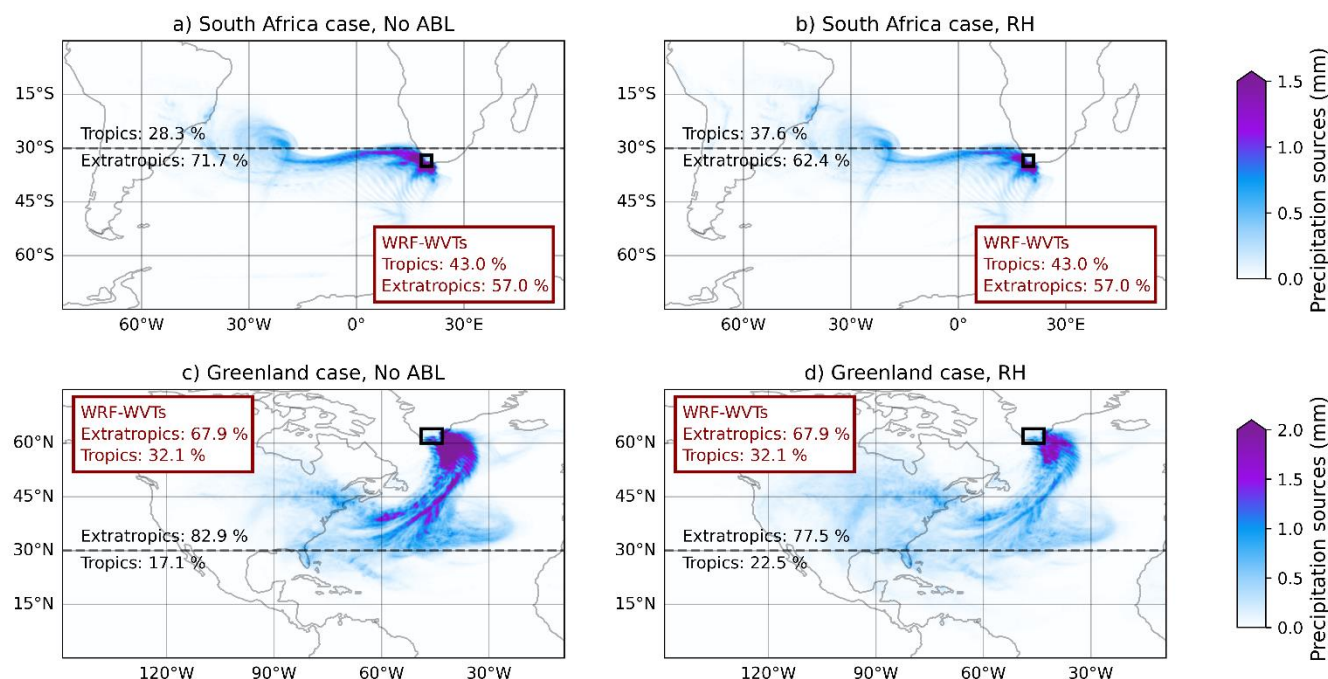
Figure 6: Precipitation sources for the South Africa (a and b), and Greenland events (c and d), computed with the WaterSip
methodology. In panels (a) and (c) the most basic configuration is used, while in panels (b) and (d) we show the results of
the "RH" configuration. The fraction of precipitation coming from the tropics and the extratropics is shown in black for each
case, and the red box shows these same contributions from WRF-WVTs.

3.2.2 UTrack

Our analysis indicated that in the case of UTrack, the underestimation of tropical contributions was notably lower than in the
WaterSip methodology, but still significant. In a similar approach to that in the previous section, we take the accuracy of the
trajectories generated by FLEXPART-WRF for granted and focus on the capabilities of the Lagrangian tool itself to
overcome this limitation. Our hypothesis now is that the way in which the air parcels to be released are selected is behind the
biases found. Given that UTrack's initial vertical distribution of particles is proportional to atmospheric humidity, parcels in
the lower troposphere are expected to play a more significant role in the UTrack calculation of moisture sources for
precipitation. However, parcels at these lower atmospheric levels hardly contribute to precipitation since they are generally
not over-saturated, i.e. they are outside the cloud level. This factor is crucial, as it is well known that moisture origin can
change greatly with altitude (e.g. Hu and Dominguez, 2019). Particles that actually contribute to precipitation could be
selected as in WaterSip, taking into account their change in specific humidity. However, Utrack only works with evaporation
and precipitable water fields, and to maintain consistency with this, we decided to use another approach, based on finding a

365 threshold height z_b, below which it is assumed that Lagrangian particles are not actually contributing to rainfall. The parcels at low levels can obviously rise if an updraft is present and end up contributing to rainfall, but this will be at later time steps, and it is then that they will be considered. Moreover, only parcels close to saturation are considered, namely, those with relative humidity higher than 90 % at this initial stage. In short, we conjecture that the basic UTrack configuration gives too much weight to the lower level air parcels, which usually contain local moisture, and hence the under-estimation of remote

370 sources. For a more technical discussion of this issue, we refer to Sect. 3.2 in the Supplement.
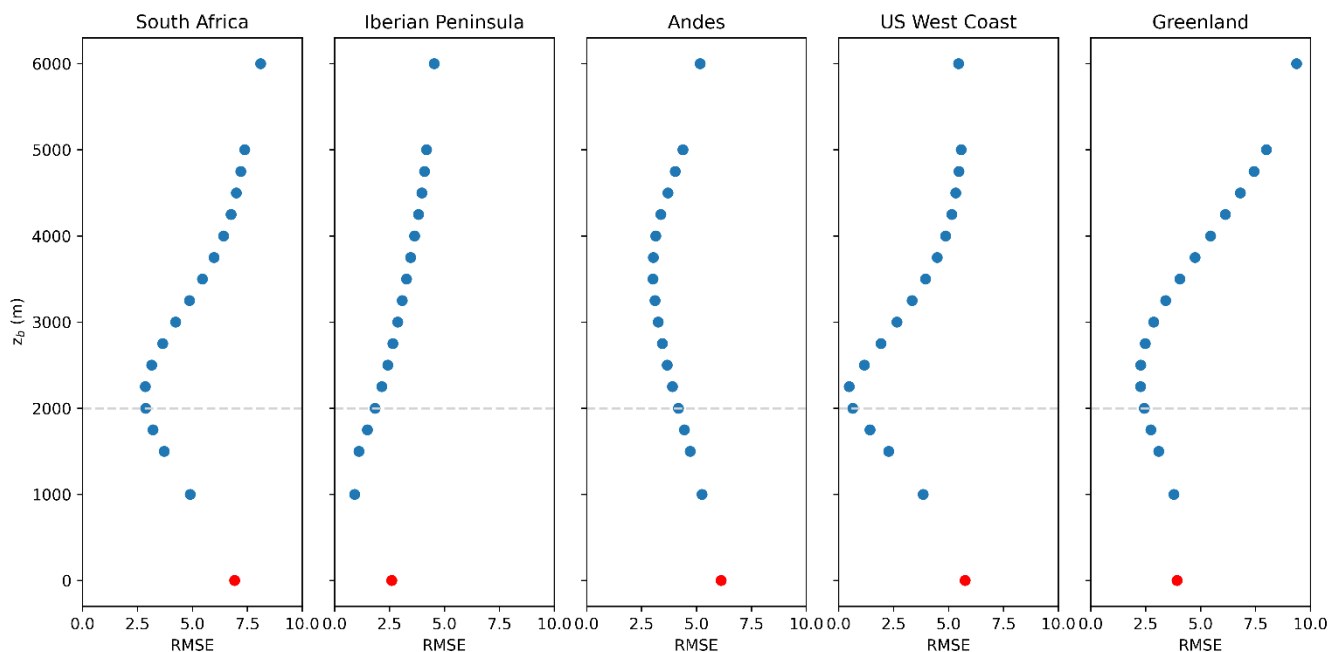
Figure 7: Variation of the RMSE with a threshold height z_b for parcel release in each AR-related rainfall event. True values are from WRF-WVTs, and predicted values are computed with UTrack, excluding parcels whose initial height is below z_b. The dashed line indicates the 2 km threshold selected. In red, the RMSE for the original UTrack configuration including all

375 parcels.

In Fig. 7 we show the variation of the RMSE with z_b for the different precipitation events. The original configuration of UTrack corresponds to the red points, i.e., $z_b = 0$ km. Our findings indicate a decrease in RMSE as z_b increases, reaching a minimum at a value that is case-dependent- Notably, for the South Africa, US West Coast and Greenland cases, the optimal

380 z_b ranges around 2 to 2.25 km, aligning with the typical lower boundary of mid-level clouds. This altitude, however, could be sensitive to the type of event, meaning that precipitation events not associated with ARs may show a different optimal threshold. The situation for the Iberian Peninsula and Andes cases is different, as the variation of the RMSE with z_b seems to follow a different pattern. Nevertheless, setting z_b to 2 km results in a decrease in RMSE for all cases, including the latter two. The maximum bias decreases by more than 50 % in the South Africa, Tropical Pacific and Greenland cases, while for

385   the Iberian Peninsula and Andes cases it is reduced by 42 % and 23 % (Fig. S8 in the Supplement). The improvement is further supported by the MAESS (Table S1 in the Supplement), as this metric is higher for all events when the proposed modifications are introduced. In some cases, such as the US West Coast, the score is exceptionally high, 0.96, indicating a strong alignment with the WRF-WVTs results. On average, the RMSE decreases from 4.64 to 2.30, while the MAESS increases from 0.77 to 0.87. Consequently, we infer that excluding parcels below 2 km in the UTrack calculation of
390   precipitation origins is a good approach to rectify the underestimation of remote sources.
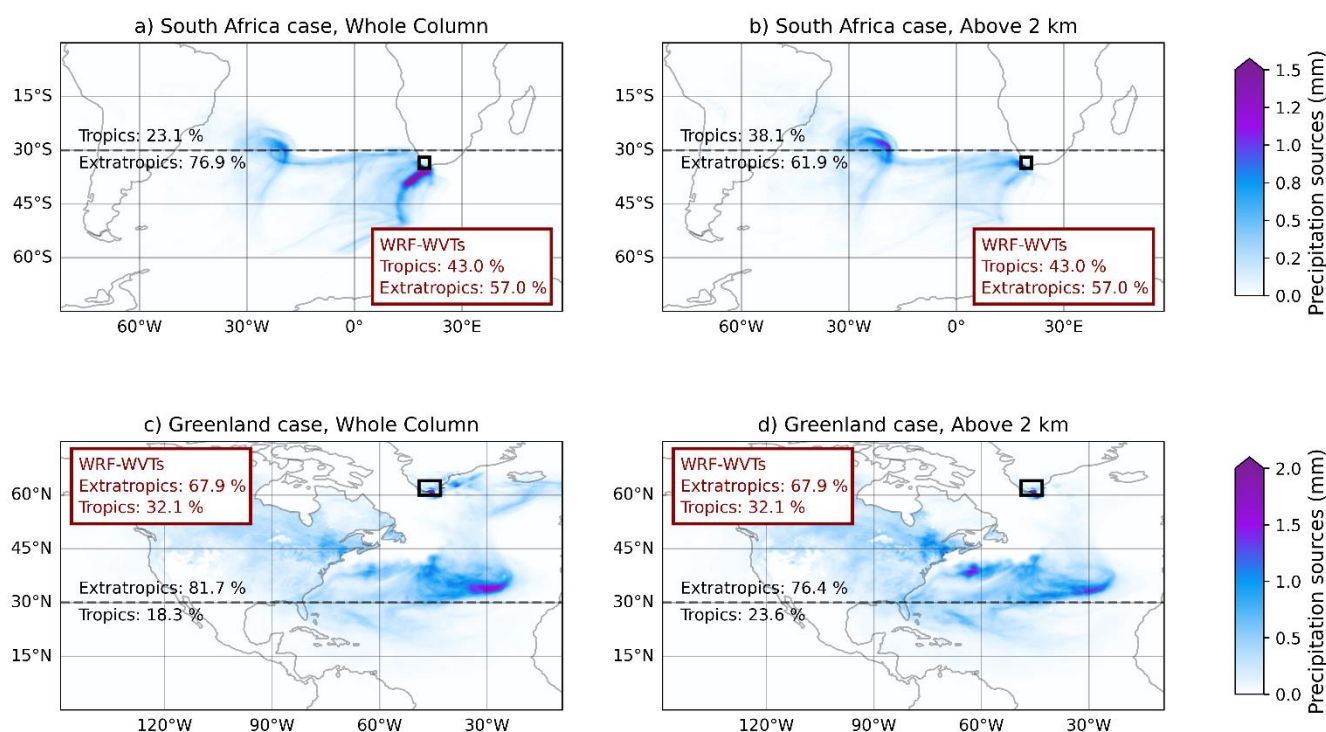
Figure 8: Precipitation sources for the South Africa (a and b), and Greenland events, (c and d), computed with UTrack. In panels a) and c) the most basic configuration is used, while in panels (b) and (d) parcels below 2 km are not considered. The fraction of precipitation coming from the tropics and the extratropics is shown in black for each case, and in the red box for
395   WRF-WVTs.

As with WaterSip, to better illustrate the comparison between the modified and unmodified versions of Utrack, we examined the spatial distribution of moisture sources for two events, the South Africa and Greenland cases. Figure 8a and c show the results from the basic configuration ("Whole Column"), where all parcels are included in the moisture sources calculation,
400   while Fig. 8b and d represent the scenario where only parcels released above 2 km are considered ("Above 2 km"). We also computed the proportions of precipitation originating from tropical and extratropical regions (black and red text in Fig. 8). In the South Africa case (top), the modified configuration ("Above 2 km") shows less intense moisture uptakes in the oceanic

area closest to the target region, indicating a reduced dominance of local sources. The latter is supported by the proportion of rainfall of tropical origin, which increases from 23.2 % to 38.1 %, closely aligning with the "true" value of 43 % provided by

405 WRF-WVTs. In the Greenland case (bottom), we can observe a reinforcement of the contributions from North America and the Tropical Atlantic when excluding parcels below 2 km. Particularly in the case of tropical contributions, there is also a significant improvement, from 18.3 % to 23.6 %, thus approaching the 32.1 % of WRF-WVTs. Obviously, as tropical contributions improve, extratropical contributions also improve for both cases. Finally, it is worth noting that the bias reduction is consistent across different sources for all cases analysed, as explicitly shown in Fig. S8 and S10 in the

410 Supplement.

3.3 Extension to ERA5

Figure 9 presents the biases in precipitation fraction for both basic and enhanced configurations of WaterSip and UTrack, with trajectories generated by the FLEXPART model using ERA5 data. Specifically, Fig. 9a and b display results for the basic configurations, analogous to those in Fig. 4, but with FLEXPART trajectories. The high correlation between both

415 figures (4 and 9) shows that the results with FLEXPART are very similar to the results with FLEXPART-WRF. As in Fig. 4, there is a clear negative bias for tropical sources and a positive bias for extratropical sources. Contrary to the results observed with FLEXPART-WRF trajectories, the basic WaterSip configuration is now better than UTrack. This is reflected in Table S3 of the Supplement, where the average RMSE of WaterSip remains almost unchanged (from 5.55 to 5.38), but that of UTrack increases significantly from 4.64 to 5.93, mainly due to a worse performance in the Iberian Peninsula and

420 Andes cases. On the other hand, Fig. 9c and d show the biases of the modified versions of WaterSip and Utrack, respectively. The improvements are again evident, as practically all biases are reduced, especially the most important ones. For instance, for WaterSip the biases in the main extratropical sources (North and South Atlantic) are reduced from 15-40 % to below 10 %. In the case of Utrack the improvements are even more remarkable, as the maximum bias goes from around 20 % to around 5 %. In terms of RMSE (Table S3 in the Supplement) the improvement for WaterSip goes from 5.38 for the

425 basic configuration to 3.25 for the modified one, and from 5.93 to 2.16 for Utrack. This improvement is also evident in terms of the MAESS (Table S3 in the Supplement). Overall, the similarity in behavior to that observed with FLEXPART-WRF outcomes suggests that our modifications are also effective when using ERA5 input data.
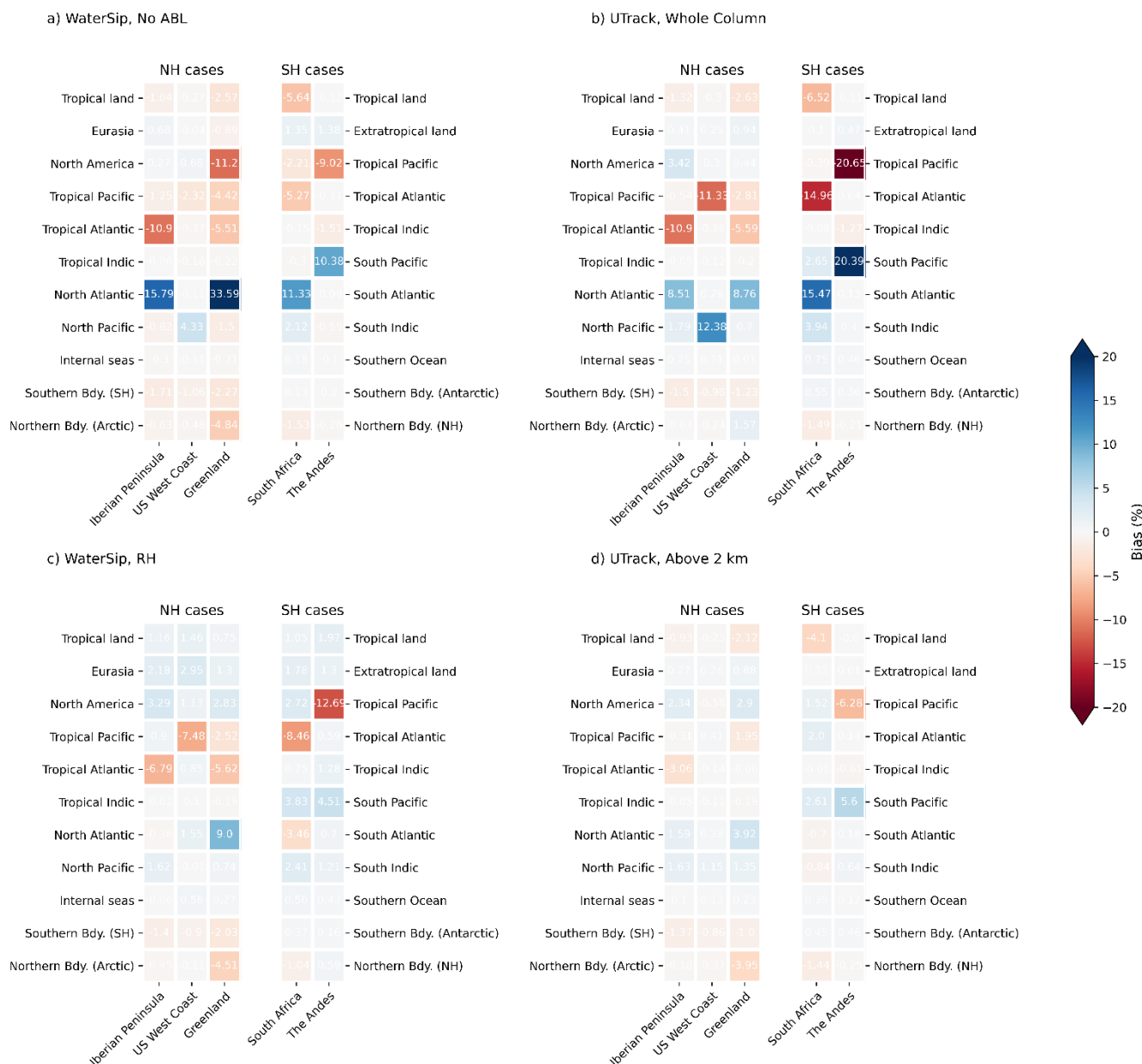
Figure 9: Bias in the precipitation fraction (%) obtained using the basic (a and b) and modified (c and d) configurations of the WaterSip (left) and UTrack (right) models, for trajectories generated with FLEXPART forced with ERA5 input data. Biases are computed subtracting the "true" outcomes of WRF-WVTs from the corresponding values of WaterSip and UTrack.

4. Summary and conclusions

In this study we have assessed the performance of WaterSip and UTrack, two of the most used Lagrangian tools for moisture

435 tracking, by comparing their results with the WRF-WVTs model in the context of AR-related precipitation events. Calculations are performed with the same WRF output data, for which WRF-WVTs results can be considered as synthetic observations. The main objective was to obtain a computationally efficient Lagrangian methodology compatible with WRF-WVTs, potentially serving as a substitute for the Eulerian technique in global or climatological applications.

440 Initially, we evaluated the most basic and commonly used configurations of WaterSip and UTrack. In the case of WaterSip, we observed important biases in the estimation of tropical and, more broadly, remote contributions, while there was an overestimation of local sources, especially of the oceanic region adjacent to where the AR makes landfall. These findings are in line with those documented in the literature (e.g. Winschall et al., 2014; Cloux et al., 2021). Quantitatively, when allowing specific humidity increments above the ABL ("No ABL" configuration), an average RMSE of 5.55 was obtained, being the

445 average skill score considered in this study (the MAESS) equal to 0.70. When not attributing these increments ("ABL" configuration), we obtained an average RMSE of 5.06 and average MAESS of 0.72. The similarity in MAESS between these configurations indicates only a minor correction in the "ABL" configuration, although for some specific cases, like the Andes case, the improvement is noteworthy. For UTrack, the initial results were slightly better, with an average RMSE of 4.64 and an average MAESS of 0.77. Despite this, there was also a remarkable underestimation of tropical contributions,

450 particularly in certain cases. These finding are also consistent with those reported in previous studies (Insua-Costa et al., 2022; Staal and Koren, 2023).

We then evaluated some physics-based modifications to try to enhance the compatibility of the results produced by WaterSip and UTrack with those of WRF-WVTs. In the case of WaterSip, we proposed not reducing previous contributions when a

455 specific humidity decrease occurs and the parcel is not close to saturation. Numerically, only decreases in specific humidity that occur when the relative humidity is above a certain threshold are considered for the calculation of moisture sources for precipitation. In the case of UTrack, as moisture sources are highly dependent on altitude, we proposed excluding from the calculations those parcels released below 2 km at the time and location of the precipitation event, trying to avoid parcels below cloud level, i.e. not contributing to rainfall. Both modifications lead to a notable improvement of the results, as the

460 average RMSE drops to 2.98 (WaterSip) and 2.30 (UTrack), so it is reduced by over 50 %. Finally, we also validated our modifications using input data from ERA5 reanalysis, the standard setting of both WaterSip and UTrack, and our results show that the proposed modifications also work well in this case.
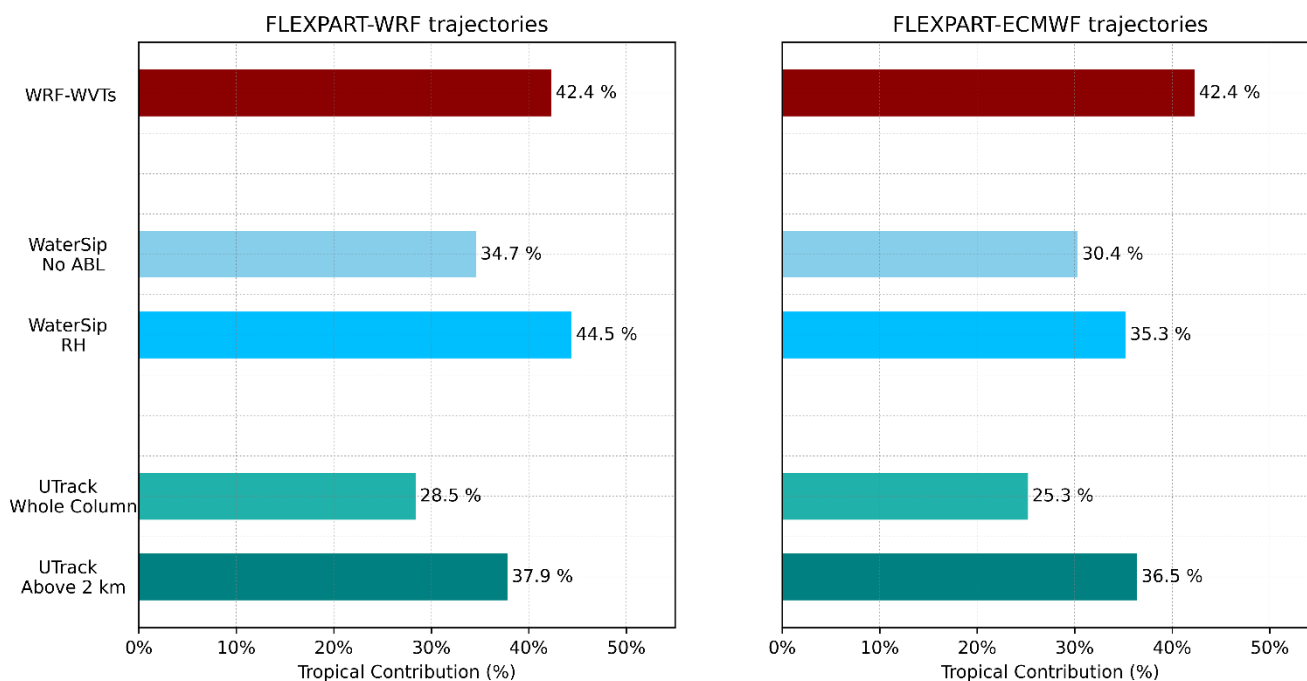
Figure 10: Average tropical contribution (%) obtained using the basic and modified configurations of the WaterSip (bluish colors) and UTrack (greenish colours), for trajectories generated with WRF input data (left) and ERA5 input data (right), in comparison with those obtained with WRF-WVTs (dark red).

Importantly, on average there is an important rectification of the underestimation of tropical contributions, as highlighted in Fig. 10. The contributions of Watersip and Utrack, which were initially in the range of 20-30 % on average, now exceed 35 %, with a maximum value of 44.5 %, very close to the WRF-WVTs 42.4 %. Therefore, after the modifications introduced, although there may be important differences for specific cases, when averaging the results for a set of cases, the conclusions drawn in terms of the partitioning of the contribution of tropical and extratropical moisture would be very similar for the three methodologies. This is particularly relevant when studying ARs, as the debate remains as to whether or not they are mostly fed by tropical moisture. Based on our findings, we conclude that these Lagrangian moisture tracking methodologies can serve as viable alternatives to WRF-WVTs or other similar methods, particularly in global or climatological studies where computational efficiency is a priority. Most interestingly, the results of the different methodologies have converged by introducing only two simple and logical (non-artificial) modifications, which suggests that further validation in the future could lead to an extraordinarily high degree of agreement between them.

480   **Data availability.** No public data are derived from this research.

Author contributions. D.I.C., E.H.G., C.L. and G.M.M. conceptualized the experiment. A.C.O. and D.I.C designed the methodology. A.C.O. performed the simulations, analyzed the data, created the figures, and wrote the first manuscript draft. D.I.C., E.H.G., C.L. and G.M.M. contributed with ideas, interpretation of the results, and manuscript revisions.

Competing interests. The authors declare that they have no conflict of interest.

485   **Acknowledgements.** Funding comes from the Spanish Ministerio de Ciencia e Innovación RIESPIRO (PID2021-128510OB-I00 to G.M.M. and A.C.O.) and LAMARCA (PID2021-123352OB-C32 to C.L. and E.H.G) projects, funded by MICIU/AEI/10.13039/501100011033 and FEDER, "Una manera de hacer Europa". D.I.C. is supported by the European Research Council (101088405, HEAT). E.H.G. and C.L. acknowledge support from the María de Maeztu project CEX2021-001164-M funded by the MICIU/AEI/10.13039/501100011033. A.C.O. acknowledges Xunta de Galicia for a predoctoral
490   grant (Programa de axudas á etapa predoutoral 2023, ED481A-2023-192). Computation took place at CESGA (Centro de Supercomputación de Galicia), Santiago de Compostela, Galicia, Spain.

References

Blamey, R. C., Ramos, A. M., Trigo, R. M., Tomé, R., and Reason, C. J. C.: The Influence of Atmospheric Rivers over the South Atlantic on Winter Rainfall in South Africa, J. Hydrometeorol., 19, 127–142, https://doi.org/10.1175/JHM-D-17-
495   0111.1, 2018.

Brioude, J., Arnold, D., Stohl, A., Cassiani, M., Morton, D., Seibert, P., Angevine, W., Evan, S., Dingwell, A., Fast, J. D., Easter, R. C., Pisso, I., Burkhart, J., and Wotawa, G.: The Lagrangian particle dispersion model FLEXPART-WRF version 3.1, Geosci. Model Dev., 6, 1889–1904, https://doi.org/10.5194/gmd-6-1889-2013, 2013.

Cloux, S., Garaboa-Paz, D., Insua-Costa, D., Miguez-Macho, G., and Pérez-Muñuzuri, V.: Extreme precipitation events in
500   the Mediterranean area: contrasting two different models for moisture source identification, Hydrol. Earth Syst. Sci., 25, 6465–6477, https://doi.org/10.5194/hess-25-6465-2021, 2021.

Dirmeyer, P. A. and Brubaker, K. L.: Contrasting evaporative moisture sources during the drought of 1988 and the flood of 1993, J. Geophys. Res. Atmospheres, 104, 19383–19397, https://doi.org/10.1029/1999JD900222, 1999.

Dominguez, F., Kumar, P., Liang, X.-Z., and Ting, M.: Impact of Atmospheric Moisture Storage on Precipitation Recycling,
505   J. Clim., 19, 1513–1530, https://doi.org/10.1175/JCLI3691.1, 2006.

Drumond, A., Marengo, J., Ambrizzi, T., Nieto, R., Moreira, L., and Gimeno, L.: The role of the Amazon Basin moisture in the atmospheric branch of the hydrological cycle: a Lagrangian analysis, Hydrol. Earth Syst. Sci., 18, 2577–2598, https://doi.org/10.5194/hess-18-2577-2014, 2014.

Eiras-Barca, J., Dominguez, F., Hu, H., Garaboa-Paz, D., and Miguez-Macho, G.: Evaluation of the moisture sources in two
510   extreme landfalling atmospheric river events using an Eulerian WRF tracers tool, Earth Syst. Dyn., 8, 1247–1261, https://doi.org/10.5194/esd-8-1247-2017, 2017.

van der Ent, R. J., Tuinenburg, O. A., Knoche, H.-R., Kunstmann, H., and Savenije, H. H. G.: Should we use a simple or complex model for moisture recycling and atmospheric moisture tracking?, Hydrol. Earth Syst. Sci., 17, 4869–4884, https://doi.org/10.5194/hess-17-4869-2013, 2013.

515 Fernández-Alvarez, J. C., Pérez-Alarcón, A., Nieto, R., and Gimeno, L.: TROVA: TRansport Of water VApor, SoftwareX, 20, 101228, https://doi.org/10.1016/j.softx.2022.101228, 2022.

Fremme, A. and Sodemann, H.: The role of land and ocean evaporation on the variability of precipitation in the Yangtze River valley, Hydrol. Earth Syst. Sci., 23, 2525–2540, https://doi.org/10.5194/hess-23-2525-2019, 2019.

Gimeno, L., Stohl, A., Trigo, R. M., Dominguez, F., Yoshimura, K., Yu, L., Drumond, A., Durán-Quesada, A. M., and
520 Nieto, R.: Oceanic and terrestrial sources of continental precipitation, Rev. Geophys., 50, https://doi.org/10.1029/2012RG000389, 2012.

Gimeno, L., Nieto, R., Vázquez, M., and Lavers, D. A.: Atmospheric rivers: a mini-review, Front. Earth Sci., 2, https://doi.org/10.3389/feart.2014.00002, 2014.

Guan, B. and Waliser, D. E.: Tracking Atmospheric Rivers Globally: Spatial Distributions and Temporal Evolution of Life
525 Cycle Characteristics, J. Geophys. Res. Atmospheres, 124, 12523–12552, https://doi.org/10.1029/2019JD031205, 2019.

Hersbach, H., Bell, B., Berrisford, P., Hirahara, S., Horányi, A., Muñoz-Sabater, J., Nicolas, J., Peubey, C., Radu, R., Schepers, D., Simmons, A., Soci, C., Abdalla, S., Abellan, X., Balsamo, G., Bechtold, P., Biavati, G., Bidlot, J., Bonavita, M., De Chiara, G., Dahlgren, P., Dee, D., Diamantakis, M., Dragani, R., Flemming, J., Forbes, R., Fuentes, M., Geer, A., Haimberger, L., Healy, S., Hogan, R. J., Hólm, E., Janisková, M., Keeley, S., Laloyaux, P., Lopez, P., Lupu, C., Radnoti, G.,
530 de Rosnay, P., Rozum, I., Vamborg, F., Villaume, S., and Thépaut, J.-N.: The ERA5 global reanalysis, Q. J. R. Meteorol. Soc., 146, 1999–2049, https://doi.org/10.1002/qj.3803, 2020.

Hu, H. and Dominguez, F.: Understanding the Role of Tropical Moisture in Atmospheric Rivers, J. Geophys. Res. Atmospheres, 124, 13826–13842, https://doi.org/10.1029/2019JD030867, 2019.

Insua-Costa, D. and Miguez-Macho, G.: A new moisture tagging capability in the Weather Research and Forecasting model:
535 formulation, validation and application to the 2014 Great Lake-effect snowstorm, Earth Syst. Dyn., 9, 167–185, https://doi.org/10.5194/esd-9-167-2018, 2018.

Insua-Costa, D., Senande-Rivera, M., Llasat, M. C., and Miguez-Macho, G.: The central role of forests in the 2021 European floods, Environ. Res. Lett., 17, 064053, https://doi.org/10.1088/1748-9326/ac6f6b, 2022.

Keune, J., Schumacher, D. L., and Miralles, D. G.: A unified framework to estimate the origins of atmospheric moisture and
540 heat using Lagrangian models, Geosci. Model Dev., 15, 1875–1898, https://doi.org/10.5194/gmd-15-1875-2022, 2022.

Koster, R., Jouzel, J., Suozzo, R., Russell, G., Broecker, W., Rind, D., and Eagleson, P.: Global sources of local precipitation as determined by the NASA/GISS GCM, Geophys Res Lett U. S., 13:1, https://doi.org/10.1029/GL013i002p00121, 1986.

Liberato, M. L. R., Ramos, A. M., Trigo, R. M., Trigo, I. F., Durán-Quesada, A. M., Nieto, R., and Gimeno, L.: Moisture Sources and Large-Scale Dynamics Associated With a Flash Flood Event, in: Geophysical Monograph Series, edited by:
545 Lin, J., Brunner, D., Gerbig, C., Stohl, A., Luhar, A., and Webley, P., American Geophysical Union, Washington, D. C., 111–126, https://doi.org/10.1029/2012GM001244, 2013.

Mattingly, K. S., Mote, T. L., and Fettweis, X.: Atmospheric River Impacts on Greenland Ice Sheet Surface Mass Balance, J. Geophys. Res. Atmospheres, 123, 8538–8560, https://doi.org/10.1029/2018JD028714, 2018.

Miguez-Macho, G., Stenchikov, G. L., and Robock, A.: Spectral nudging to eliminate the effects of domain position and
550   geometry in regional climate model simulations, J. Geophys. Res. Atmospheres, 109, https://doi.org/10.1029/2003JD004495,
2004.

Oki, T. and Kanae, S.: Global Hydrological Cycles and World Water Resources, Science, 313, 1068–1072,
https://doi.org/10.1126/science.1128845, 2006.

Pisso, I., Sollum, E., Grythe, H., Kristiansen, N. I., Cassiani, M., Eckhardt, S., Arnold, D., Morton, D., Thompson, R. L.,
555   Groot Zwaaftink, C. D., Evangeliou, N., Sodemann, H., Haimberger, L., Henne, S., Brunner, D., Burkhart, J. F., Fouilloux,
A., Brioude, J., Philipp, A., Seibert, P., and Stohl, A.: The Lagrangian particle dispersion model FLEXPART version 10.4,
Geosci. Model Dev., 12, 4955–4997, https://doi.org/10.5194/gmd-12-4955-2019, 2019.

Ralph, F. M., Neiman, P. J., Wick, G. A., Gutman, S. I., Dettinger, M. D., Cayan, D. R., and White, A. B.: Flooding on
California's Russian River: Role of atmospheric rivers, Geophys. Res. Lett., 33, https://doi.org/10.1029/2006GL026689,
560   2006.

Ramos, A. M., Nieto, R., Tomé, R., Gimeno, L., Trigo, R. M., Liberato, M. L. R., and Lavers, D. A.: Atmospheric rivers
moisture sources from a Lagrangian perspective, Earth Syst. Dyn., 7, 371–384, https://doi.org/10.5194/esd-7-371-2016,
2016.

Rios-Entenza, A. and Miguez-Macho, G.: Moisture recycling and the maximum of precipitation in spring in the Iberian
565   Peninsula, Clim. Dyn., 42, 3207–3231, https://doi.org/10.1007/s00382-013-1971-x, 2014.

Skamarock, C., Klemp, B., Dudhia, J., Gill, O., Liu, Z., Berner, J., Wang, W., Powers, G., Duda, G., Barker, D., and Huang,
X.: A Description of the Advanced Research WRF Model Version 4.3, https://doi.org/10.5065/1dfh-6p97, 2021.

Sodemann, H. and Stohl, A.: Asymmetries in the moisture origin of Antarctic precipitation, Geophys. Res. Lett., 36,
https://doi.org/10.1029/2009GL040242, 2009.

570   Sodemann, H., Schwierz, C., and Wernli, H.: Interannual variability of Greenland winter precipitation sources: Lagrangian
moisture diagnostic and North Atlantic Oscillation influence, J. Geophys. Res. Atmospheres, 113, D03107,
https://doi.org/10.1029/2007JD008503, 2008.

Staal, A. and Koren, G.: Comment on 'The central role of forests in the 2021 European floods,' Environ. Res. Lett., 18,
048002, https://doi.org/10.1088/1748-9326/acc260, 2023.

575   Stohl, A. and James, P.: A Lagrangian Analysis of the Atmospheric Branch of the Global Water Cycle. Part I: Method
Description, Validation, and Demonstration for the August 2002 Flooding in Central Europe, J. Hydrometeorol., 5, 656–678,
https://doi.org/10.1175/1525-7541(2004)005<0656:ALAOTA>2.0.CO;2, 2004.

Trenberth, K. E.: Atmospheric Moisture Recycling: Role of Advection and Local Evaporation, J. Clim., 12, 1368–1381,
https://doi.org/10.1175/1520-0442(1999)012<1368:AMRROA>2.0.CO;2, 1999.

580   Tuinenburg, O. A. and Staal, A.: Tracking the global flows of atmospheric moisture and associated uncertainties, Hydrol.
Earth Syst. Sci., 24, 2419–2435, https://doi.org/10.5194/hess-24-2419-2020, 2020.

Viale, M., Houze, R. A., and Rasmussen, K. L.: Upstream Orographic Enhancement of a Narrow Cold-Frontal Rainband
Approaching the Andes, Mon. Weather Rev., 141, 1708–1730, 2013.

Winschall, A., Pfahl, S., Sodemann, H., and Wernli, H.: Comparison of Eulerian and Lagrangian moisture source diagnostics
585 – the flood event in eastern Europe in May 2010, Atmospheric Chem. Phys., 14, 6605–6619,
https://doi.org/10.5194/acp-14-6605-2014, 2014.